Energy Proceedings
Vol 50, 2025
ISSN 2004-2965

Numerical study on flow field structure of anion exchange membrane electrolysis cell based on heat transfer-mass transfer- electron conduction#

Yanjun Chen[1,2,3], Wenjia Li[4*], Juan Song[1,2,3], Zongkang Wang[1,2,3], Zhenyu Tian[1,2,3*]
1 Key Laboratory of Efficient Utilization of Low and Medium Grade Energy, Tianjin University, Tianjin, 300350, PR China
2 School of Mechanical Engineering, Tianjin University, Tianjin, 300072, PR China
3 National Industry-Education Platform of Energy Storage, Tianjin University, Tianjin, 300350, PR China
4 South University of Science and Technology, Shenzhen, 518055, PR China
(Corresponding Author: tianzhenyu@tju.edu.cn)

ABSTRACT

Bipolar plates are integral to the functionality of anion exchange membrane electrolysis cells, with the flow field design being a critical determinant of heat and mass transfer, as well as electron conduction within the cell. This paper establishes a simulation model for anion exchange membrane electrolysis cells and analyzes the influence of the geometric structure of the serpentine flow field on the performance of the electrolysis cells based on the trade-off relationship between heat transfer, mass transfer, electron conduction. The results indicate that the dominant factors affecting current density when changing the channel width are electron potential and temperature. The smaller the channel width, the higher the electron potential and temperature, and the higher the current density. When the changing factor is the number of inlets in the flow field, the higher the liquid saturation, the higher the current density. Therefore, the current density is ranked as follows: 1-path serpentine flow field >3-path serpentine flow field >2-path serpentine flow field. Therefore, when the voltage is 2 V, the 1-path serpentine flow field with a channel width of 0.6 mm has the highest current density, which is 10.8% higher than the 2-path serpentine flow field with the lowest current density.

Keywords: anion exchange membrane electrolysis cell, simulation of multi-physical field coupling, serpentine flow field, electron conduction, heat and mass transfer

NONMENCLATURE

Abbreviations	
AEMEC	Anion Exchange Membrane Electrolysis Cell
APTL	Anode Porous Transport Layer
ACL	Anode Catalyst Layer
AEM	Anion Exchange membrane
Symbols	
σ	Conductivity
φ_{s}	Electron potential
φ_{ion}	Electrolyte potential
s	Liquid saturation
ε	Porosity
K	Permeability

1. INTRODUCTION

Hydrogen, as an energy carrier, has the characteristics of pollution-free and high energy density. It can be coupled with renewable energy to achieve energy storage and solve the problem of unstable renewable energy supply [1]. Water electrolysis has the characteristics of high efficiency and environmental protection, and is one of the most anticipated hydrogen production technologies [2]. In water electrolysis, the anion exchange membrane electrolysis cell can produce high-purity hydrogen with high efficiency, while also being adaptable to fluctuating renewable energy sources and flexible peak shaving.

Bipolar plates play a crucial role in electrolysis cells [3]. Optimizing its geometric parameters is an important method to enhance mass transport and heat transfer, and promote electron conduction. However, the complex trade-off relationships between heat transfer-mass transfer- electron conduction within AEMEC make it difficult to optimize the flow field structure of AEMEC [4]. In electrolysis cells, sufficient reactants are beneficial for the reaction to proceed, but the raw material of the electrolysis cells is liquid. Strengthening the liquid supply will cause a decrease in the temperature of the reaction zone, which will have adverse effects. At the same time, in order to reduce the ohmic impedance of the electrolysis cells, it is necessary to arrange the position of the flow channels and ribs reasonably. However, the flow field form that is conducive to electron conduction may not be conducive to fluid flow. For example, Zhang et al. [5] and Zhuang et al. [6] both found that in PEMEC, the

This is a paper for the 16th International Conference on Applied Energy (ICAE2024), Sep. 1-5, 2024, Niigata, Japan.

thinner the flow channel, the better the electrochemical performance of the electrolysis cells. However, they only analyzed the favorable effects of the dominant factor - the enhanced electron transport, and did not fully analyze and discuss the unfavorable effects of the non dominant factor - the deteriorated transport of reactants. In fact, the analysis of the trade-off relationship between heat transfer, mass transfer, and conductivity is essential because analyzing the trade-off relationship can provide direction for increasing the positive impact of dominant factors and reducing the negative impact of non dominant factors, thereby improving the performance of electrolytic cells from two aspects.

Therefore, in this paper, a 3D, two-phase flow, non isothermal, pure water based model is established for AEMEC, and then the influence of the geometric structure of the serpentine flow field on the performance of the electrolyzer is explored. Furthermore, it scrutinizes the trade-off relationships between mass transport, heat transfer, and electron conduction, and their collective influence on the electrochemical performance.

2. NUMERICAL MODEL

2.1 Physical model

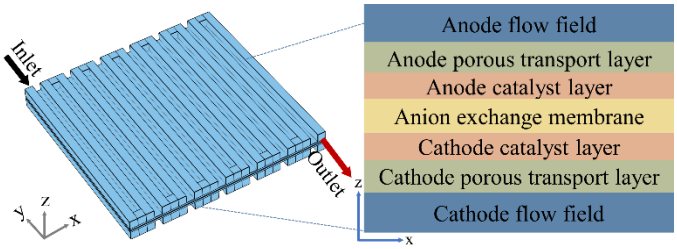

Fig. 1 The computational domain of the AEMEC

The computational domain of the AEMEC is shown in Fig.1. AEMEC consists of anode flow field, anode porous transport layer, anode catalyst layer, anion exchange membrane, cathode catalyst layer, cathode porous transport layer, and cathode flow field. The geometric parameters of AEMEC are shown in Table 1. To promote the release of generated gases and prevent membrane dehydration, water is supplied to the anode and cathode. The water entering the anode flow field inlet is transported through APTL and reaches ACL. In ACL, OH^- is consumed to generate oxygen and water. Afterwards, the mixture of oxygen and water products passes through ACL and APTL in sequence and flows out from outlet. In CCL, water receives electrons conducted from external circuits to generate hydrogen and OH^-. The generated OH^- is transported through the AEM from the cathode to the anode under the action of electroosmotic resistance, and the mixture of hydrogen and water produced flows out from the outlet.

The serpentine flow field is a commonly used form of flow field. Fig.2 shows five different serpentine flow fields compared and analyzed in this paper. Case 1, case 2, and case 3 are 1-path serpentine flow fields with channel widths of 0.6 mm, 0.8 mm, and 1 mm, respectively. Case 4 is a 2-path serpentine flow field with a channel width of 1 mm. Case 5 is a 3-path serpentine flow field with a channel width of 1 mm.

Table 1 Geometric parameters of AEMEC

Parameter	Value
Channel width/channel height/rib width	1/1/1 mm
Thickness of APTL/ACL/CCL/CPTL	0.20/0.01/0.01/0.20 mm
Thickness of AEM	0.07 mm
Length/width of flow field	25/25 mm

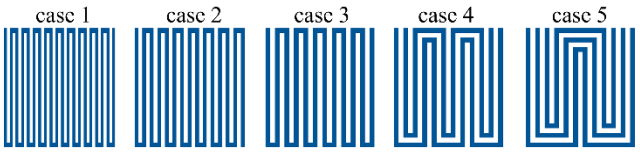

Fig 2 Five different serpentine flow fields

2.2 Assumption

(1) The fluid is considered an incompressible fluid, and the flow form is laminar flow. [7, 8]

(2) Ignore the ohmic loss caused by contact impedance between components.

(3) The catalyst layer, porous transport layer, and membrane are considered uniform and isotropic.

(4) The flow field plate has a high conductivity, so in order to accelerate the calculation speed, the calculation domain does not include the flow field plate solid.

2.3 Governing equations and boundary conditions

Table 2 shows the main equations used in this paper. Set a constant voltage V_{cell} at the interface between the anode flow field plate ribs and APTL, and a constant voltage of 0 V at the interface between the cathode flow field plate ribs and CPTL. The inlet water velocity of the anode and cathode flow fields is 0.1 m/s. The outlets of the anode and cathode flow fields are set as atmospheric pressure outlets. The inlet water temperature is 343.15 K. The liquid saturation at the inlet is set to 0.9. Table 3 shows the parameters used in the equations.

Table 2 Governing equations

Description	Expression[9]
Mass	$\nabla\cdot\left(\rho_{l/g}\overrightarrow{u_{l/g}}\right)=S_{l/g}$
Momentum	$\frac{\rho_{l/g}}{\varepsilon^{\text{eff}}}\left(\overrightarrow{u_{l/g}}\cdot\nabla\right)\frac{\overrightarrow{u_{l/g}}}{\varepsilon^{\text{eff}}}$ $=\nabla\cdot\left[-p_{l/g}\bar{\bar{I}}+\frac{\mu_{l/g}}{\varepsilon^{\text{eff}}}\left(\nabla\overrightarrow{u_{l/g}}+\left(\nabla\overrightarrow{u_{l/g}}\right)^{T}\right)\right.$ $\left.-\frac{2}{3}\frac{\mu_{l/g}}{\varepsilon^{\text{eff}}}\left(\nabla\cdot\overrightarrow{u_{l/g}}\right)\bar{\bar{I}}\right]-\left(\frac{\mu_{l/g}}{K_0K_{rl/g}}+\frac{S_{l/g}}{\left(\varepsilon^{\text{eff}}\right)^2}\right)\overrightarrow{u_{l/g}}$
Liquid saturation	$\nabla\cdot\left(-\rho_g D_c\nabla s_l+\rho_g\frac{K_{rg}\mu_l}{K_{rl}\mu_g}\vec{u}_l\right)=S_g$ $D_c=\frac{\sigma\cos\theta}{\mu_g}K_{rg}\left(\varepsilon K_0\right)^{0.5}\frac{dJ\left(s_l\right)}{ds_l}$
Charge	$\nabla\cdot\left(-\sigma_s\nabla\varphi_s\right)=R_s\ \nabla\cdot\left(-\sigma_{ion}\nabla\varphi_{ion}\right)=R_{ion}$
Energy	$\nabla\cdot\left(\rho_{\text{eff}}C_{p,\text{eff}}\vec{u}T\right)=\nabla\cdot\left(k_{\text{eff}}T\right)+S_T$
Butler-Volmer	ACL： $R=s_l^{\omega}a_{v,a}j_{an}\left(\text{e}^{\frac{\alpha_{an}^{a}F\eta_{an}}{R_cT}}-\text{e}^{\frac{-\alpha_{an}^{c}F\eta_{an}}{R_cT}}\right)$ CCL： $R=s_l^{\omega}a_{v,c}j_{cat}\left(-\text{e}^{\frac{\alpha_{cat}^{a}F\eta_{cat}}{R_cT}}+\text{e}^{\frac{-\alpha_{cat}^{c}F\eta_{cat}}{R_cT}}\right)$ $j_{an}=j_{ref,an}\exp\left(\frac{-E_a}{R_c}\left(\frac{1}{T}-\frac{1}{T_{ref}}\right)\right)$ $j_{cat}=j_{ref,cat}\exp\left(\frac{-E_c}{R_c}\left(\frac{1}{T}-\frac{1}{T_{ref}}\right)\right)$

Table 3 Main parameters in the equations

Parameter	Value
APTL/ACL/CCL/CPTL porosity	0.6/0.5/0.5/0.6
APTL/ACL/CCL/CPTL permeability	6.2×10^{-12}/6.2×10^{-13} /6.2×10^{-13}/6.2×10^{-12} m^2
Contact angle	80°

3. RESULTS AND DISCUSSION

3.1 Model validation

Fig.3 shows the variation of current density and relative error with the number of grids. It can be seen from the figure that when the number of grids reaches 350 thousand, the relative error of current density is less than 0.01%. Therefore, the number of grids used is 350 thousand. The number of grids used in all cases in this paper is after grid independence verification. Fig.4 shows the comparison between simulation results and experimental results [10]. Through the comparison, it can be seen that the numerical model established in this paper is basically accurate.

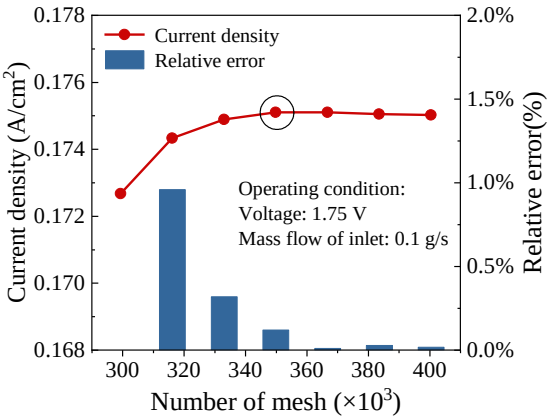

Fig. 3 Mesh independence verification

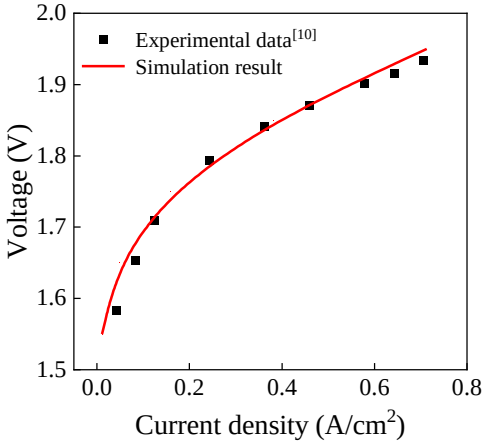

Fig. 4 Comparison of simulated and experimental data

3.2 Comparison of Electrochemical performance

Fig.5 shows the current density of different flow fields. It can be seen that at any voltage, the order of current density is: case 1>case 2>case 3>case 5>case 4. For example, when the voltage is 2 V, the current density of case 1 is 1.03 A/cm^2, case 2 is 0.99 A/cm^2, case 3 is 0.937 A/cm^2, case 4 is 0.93 A/cm^2, and case 5 is 0.935 A/cm^2. The current density of case 1 is 10.8% higher than that of case 4. Among the three flow fields of case 1, case 2, and case 3, case 1 has the highest current density, followed by case 2, and finally case 3. This is because case 1 has the smallest channel width. Therefore, it has the most densely distributed ribs, which improves the conductivity

of PTL along the plane direction and results in the highest current density. The reasons for the differences in current density of case 3, case 4, and case 5 are described in the following text.

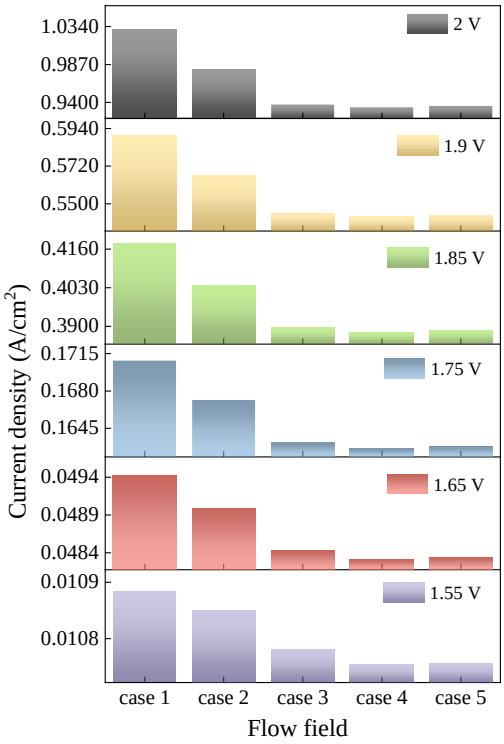

Fig. 5 Comparison of electrochemical performance

3.3 Comparison and analysis of heat and mass transfer characteristics and electron conductivity

Fig.6 shows the liquid saturation of different flow fields. It can be seen from the figure that at any voltage, the order of ACL liquid saturation in case 1, case 2, and case 3 flow fields is: case 1<case 2<case 3. For example, when the voltage is 2 V, the liquid saturation of case 1 is 0.628, the liquid saturation of case 2 is 0.631, and the liquid saturation of case 3 is 0.632. From case 1 to case 3, the liquid saturation increases by 0.004. This is because case 1 has the highest current density and produces the most oxygen in ACL, resulting in the lowest liquid saturation. Due to the current density being ranked as case 1>case 2>case 3, the liquid saturation is ranked as case 1<case 2<case 3. In addition, from Fig. 6, it can be seen that at any voltage, the order of liquid saturation for case 3, case 4, and case 5 is: case 3>case 5>case 4.

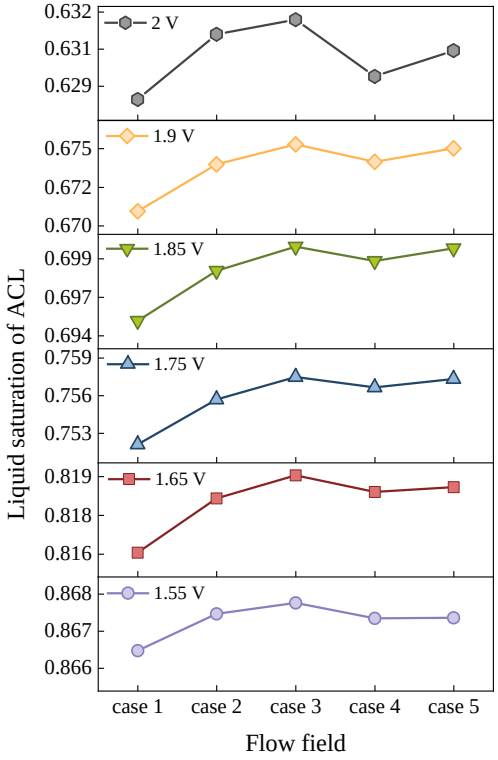

Fig. 6 Comparison of liquid saturation

Fig.7 shows the temperature variation of ACL. It can be seen that when the voltage is 1.55 V, the temperature of ACL under five flow fields is 343.16 K. As the voltage increases, the ACL temperature under each flow field begins to show differences. When the voltage is 1.65 V, the temperature of ACL for case 1, case 2, and case 3 is 343.27 K, and the temperature of ACL for case 4 and case 5 is 343.26 K. When the voltage is 1.75 V, 1.85 V, and 1.9 V, the order of temperature is: case 1>case 2>case 3>case 4=case 5. When the voltage further increases to 2 V, the order of ACL temperature is: case 1>case 2>case 3>case 4>case 5. Changing from case 5 to case 1, the temperature increases from 350.68 K to 351.29 K. The temperature ranking of ACL varies with different voltages because temperature is influenced by multiple factors. On the one hand, the higher the current density, the more ohmic heat is generated and the higher the temperature; On the other hand, the higher the liquid saturation, the lower the temperature. Multiple factors work together to cause temperature sorting to vary with different voltages. When the voltage is 1.75 V, 1.85 V, 1.9 V, and 2 V, the difference in ACL temperature between case 1, case 2, and case 3 is mainly caused by ohmic heat generated by current density. Therefore, the temperature order is: case 1>case 2>case 3. The difference in temperature among case 3, case 4, and case 5 is caused by the trade-off between ohmic heat and liquid saturation. For example, when the voltage is 2 V,

the current density in case 5 is slightly higher than that in case 4, resulting in slightly more ohmic heat. However, the liquid saturation of ACL in case 5 is higher than that in case 4, which will cause a decrease in temperature. As a result of both factors, the ACL temperature in case 5 is lower than that in case 4.

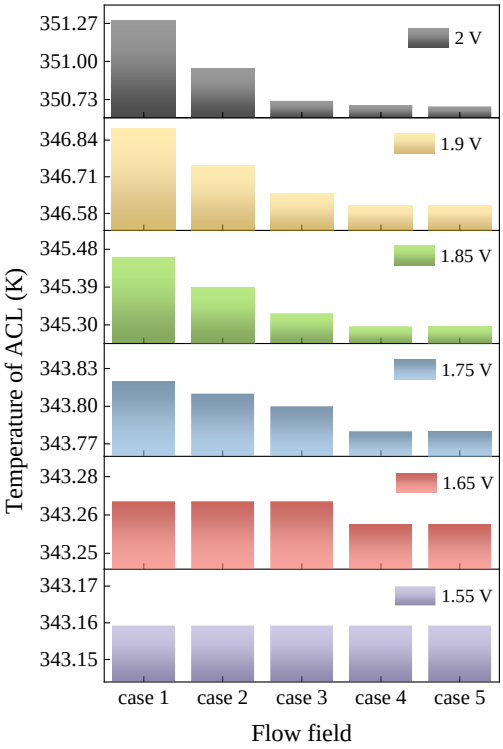

Fig. 7 Comparison of temperature

In this study, constant voltage boundary conditions are adopted, s_l, $\exp\left(-E_a / R_c \times \left(1/T - 1/T_{ref}\right)\right)$ and η_{an}/T were used to positively correlate the electrochemical reaction rate. Therefore, in order to thoroughly analyze the reasons for the differences in current density among the five flow fields, various potentials within the ACL were analyzed. Fig. 8 shows the potential analysis at a voltage of 2 V. It can be seen that the order of electron potential φ_s is case 1>case 2>case 3>case 5>case 4. The maximum electron potential in case 1 is due to its dense and uniform rib distribution, and enhanced conductivity of PTL along the plane direction. The order of electrolyte potential is: case 1>case 2>case 3>case 5>case 4; The order of equilibrium potential is: case 5>case 4>case 3>case 2>case 1. The overpotential η_{an} is influenced by electron potential, electrolyte potential, and equilibrium potential: the larger the electron potential, the smaller the electrolyte potential, and the smaller the equilibrium potential, the larger the overpotential η_{an}. Therefore, the order of overpotential magnitude is: case 1>case 2>case 3>case 5>case 4. In case 1, the rib distribution is dense and uniform, and the enhancement of PTL conductivity along the plane direction is the fundamental reason for the increase in overpotential η_{an}.

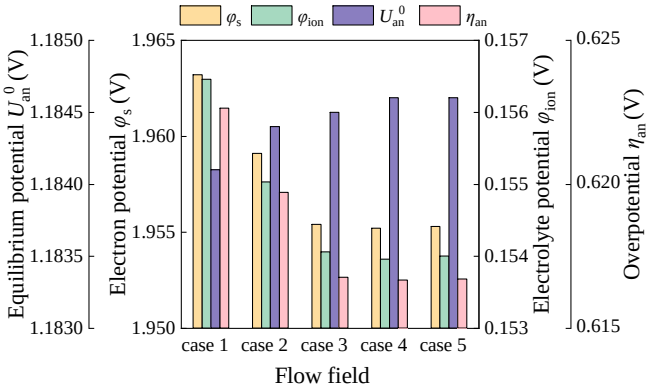

Fig. 8 V_{cell}=2 V, potential analysis of ACL

To directly analyze the causes of changes in current density, Fig.9 shows the electrochemical reaction rate analysis at a voltage of 2 V. It can be seen that the trend of η_{an}/T and $\exp\left(-E_a / R_c \times \left(1/T - 1/T_{ref}\right)\right)$ are the same as the change trend of current density in case 1, case 2, and case 3 in Fig. 5. However, from Fig.5 and Fig.6, it can be found that the trend of liquid saturation in case 1, case 2, and case 3 is completely opposite to the trend of current density. This indicates that the changes in current density in case 1, case 2, and case 3 are dominated by temperature and electron potential. Case 1 has the highest current density because it has the highest temperature and the highest electron potential. Essentially, it is because case 1 has the smallest channel width and the channels and ribs are densely and uniformly distributed, which improves its conductivity along the plane direction, increases temperature, and current density. The difference in current density between case 3, case 4, and case 5 is mainly affected by the liquid saturation. As the ACL liquid saturation is ranked as case 3>case 5>case 4, the current density is ranked as case 3>case 5>case 4.

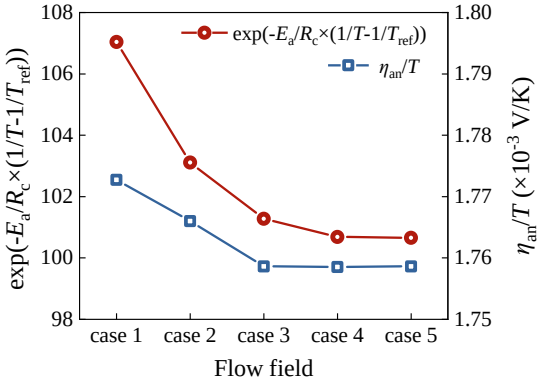

Fig. 9 V_{cell}=2 V, analysis of electrochemical reaction rate

Therefore, from the above analysis, it can be found that there is a trade-off relationship between heat transfer, mass transfer and electron conduction when changing the channel width. From case 3 to case 1, electron transport within the PTL plane is promoted, current density increases, and temperature rises; The increase in current density leads to an increase in gas production, which covers the active sites of the catalyst layer, resulting in a decrease in liquid saturation in the catalyst layer, deterioration of reactant transport. However, due to the dominant effect is electron conduction, the influence of liquid saturation is a secondary factor. Therefore, as the channel width decreases, the current density increases. When the number of inlets in the flow field changes, due to the influence of liquid saturation, the order of ACL liquid saturation is: case 3>case 5>case 4, so the order of current density is: case 3>case 5>case 4.

4. CONCLUSION

This paper establishes a model of AEMEC, and explores the influence of serpentine flow field structure on the performance of electrolyzer. When changing the width of the flow channel, the dominant factors affecting current density are electron potential and temperature. The higher the electron potential, and the higher the temperature, the greater the current density. Although liquid water saturation has an impact on current density, its effect is relatively small. Therefore, the relationship between current density is: case 1>case 2>case 3. When the changing factor is the number of inlets, that is, comparing case 3, case 4, and case 5, the higher the liquid saturation, the higher the current density, so the current density is ranked as: case 3>case 5>case 4. In five types of serpentine flow fields, when the voltage is 2 V, case 1 has a current density of 1.03 A/cm^2, which is 10.8% higher than case 4.

ACKNOWLEDGEMENT

This study was supported by the National Natural Science Foundation of China (No. 52293414).

REFERENCE

[1] Sazali N. Emerging technologies by hydrogen: A review. International Journal of Hydrogen Energy. 2020;45:18753-71.

[2] Liu Z, Sun Y, Xing C, Liu J, He Y, Zhou Y, et al. Artificial intelligence powered large-scale renewable integrations in multi-energy systems for carbon neutrality transition: Challenges and future perspectives. Energy and AI. 2022;10:100195.

[3] Bazarah A, Majlan EH, Husaini T, Zainoodin AM, Alshami I, Goh J, et al. Factors influencing the performance and durability of polymer electrolyte membrane water electrolyzer: A review. International Journal of Hydrogen Energy. 2022;47:35976-89.

[4] Kerkoub Y, Benzaoui A, Haddad F, Ziari YK. Channel to rib width ratio influence with various flow field designs on performance of PEM fuel cell. Energy Conversion and Management. 2018;174:260-75.

[5] Zhang Z, Xing X. Simulation and experiment of heat and mass transfer in a proton exchange membrane electrolysis cell. International Journal of Hydrogen Energy. 2020;45:20184-93.

[6] Zhuang Y, Cui P, Long R, Liu W, Liu Z. Multi-objective optimization of channel structure for a proton exchange membrane water electrolysis cell. International Journal of Hydrogen Energy. 2024;49:337-52.

[7] Chen Z, Wang X, Liu C, Gu L, Yin L, Xu C, et al. Numerical investigation of PEM electrolysis cell with the new interdigitated-jet hole flow field. International Journal of Hydrogen Energy. 2022;47:33177-94.

[8] Jiang Y, Li Y, Ding Y, Hu S, Dang J, Yang F, et al. Simulation and experiment study on two-phase flow characteristics of proton exchange membrane electrolysis cell. Journal of Power Sources. 2023;553.

[9] Zhou H, Meng K, Chen W, Chen B. Exploratory research on bubbles migration behavior and mass transfer capacity evaluation of proton exchange membrane water electrolyzer based on a volume of fluid-coupled electrochemical model. Energy Conversion and Management. 2023;290.

[10] Xiao L, Zhang S, Pan J, Yang C, He M, Zhuang L, et al. First implementation of alkaline polymer electrolyte water electrolysis working only with pure water. Energy & Environmental Science. 2012;5.